

## Article

# Tribological Properties of Multilayer DLC/MoS<sub>2</sub> Nanocomposite Coatings on Microtextured Titanium Alloy Surfaces

Ke Liu <sup>1,2</sup>, Qingqing Ding <sup>3</sup>, Hao Peng <sup>1,2</sup>, Kang Guan <sup>1,2</sup>, Xiaowan Xi <sup>1,2</sup>, Ning Kong <sup>3,\*</sup>  and Maolin Liao <sup>3</sup>

<sup>1</sup> CNPC Engineering Technology R & D Company Limited, Beijing 102206, China; liukedr@cnpc.com.cn (K.L.); penghaodri@cnpc.com.cn (H.P.); gkangdri@cnpc.com.cn (K.G.); xixiaowandr@cnpc.com.cn (X.X.)

<sup>2</sup> National Engineering Research Center of Oil & Gas Drilling and Completion Technology, Beijing 102206, China

<sup>3</sup> School of Mechanical Engineering, University of Science and Technology Beijing, Beijing 100083, China; m202220565@xs.ustb.edu.cn (Q.D.); liaomaolin@ustb.edu.cn (M.L.)

\* Correspondence: kongning@ustb.edu.cn

**Abstract:** Single surface texture or coating technology is gradually unable to produce lasting lubrication of a TC4 titanium alloy in a harsh environment. In order to address this problem, a rectangular microstructure is prepared on the surface of a TC4 titanium alloy by laser processing, and then MoS<sub>2</sub>/DLC composite interlayer nanocoatings are prepared on the surface by non-equilibrium magnetron sputtering. Friction and wear tests are then carried out on single fabricated, coated and fabricated coatings. The results show that the MoS<sub>2</sub>/DLC composite interlayered nanocoating can effectively combine with the texture to achieve better friction reduction compared with the single texture and coating. The textured composite coating has the lowest friction coefficient (reduced from 0.4122 to 0.0978) and wear. Through controlled experiments, the textured coating showed good tribological properties at different temperatures and in different friction cycle tests. This study can effectively improve the tribological properties of metal materials through composite coatings, providing research ideas for enhancing the service life of alloys under long-term friction in high-temperature environments.

**Keywords:** microtexture; composite coating; friction properties; synergy



**Citation:** Liu, K.; Ding, Q.; Peng, H.; Guan, K.; Xi, X.; Kong, N.; Liao, M. Tribological Properties of Multilayer DLC/MoS<sub>2</sub> Nanocomposite Coatings on Microtextured Titanium Alloy Surfaces. *Lubricants* **2024**, *12*, 374. <https://doi.org/10.3390/lubricants12110374>

Received: 10 October 2024  
Revised: 22 October 2024  
Accepted: 24 October 2024  
Published: 29 October 2024



**Copyright:** © 2024 by the authors. Licensee MDPI, Basel, Switzerland. This article is an open access article distributed under the terms and conditions of the Creative Commons Attribution (CC BY) license (<https://creativecommons.org/licenses/by/4.0/>).

## 1. Introduction

Surface texturing and surface coating technologies have become two major methods to improve the tribological properties of materials. Among them, microtexturing is developed by bionic technology [1–3], which can utilize non-smooth textures to store the lubricant and realize secondary lubrication, store abrasive debris to reduce abrasive wear and generate a dynamic pressure effect to form dynamic pressure lubrication, thus effectively reducing friction and wear generation [4–6]. Solid coating technology, using the low shear characteristics of the coating itself, has a very low coefficient of friction [7–9] to achieve friction reduction lubrication. Compared with traditional liquid lubrication or grease lubrication, solid lubricant coatings have better wear resistance, a longer service life and can adapt to extreme temperatures and environments [10].

Diamond-like carbon (DLC) is a general term for a class of amorphous carbon films containing diamond structures (sp<sup>3</sup> hybrid bonds) and graphite structures (sp<sup>2</sup> hybrid bonds), which have low friction coefficients, high hardness and wear resistance [11–13], and ENKE [14] et al. first reported that diamond-like films have extremely low friction coefficients in 1980. DLC has been widely researched and applied in the field of solid lubricating coatings due to its excellent tribological properties. Dimigen first introduced metal-containing DLC (Me-DLC) into tribological applications in 1983 [15], and it was found that the mechanical properties of DLC films can be altered by controlling the concentration and type of different elements in the film [16,17]. Ajayi et al. [18] studied the tribological

properties of Si-doped DLC films in different environments, and the appropriate amount of Si-doped films in a high vacuum environment resulted in a friction coefficient as low as 0.007. Gassner et al. [19,20] showed that by controlling the size and distribution of CrC nanoparticles in the film, the film exhibits a low friction factor and good wear resistance. With the deepening of the research on solid coatings, the performance is improved by doping compounds in DLC films, which opens up a new direction for the research of DLC coatings. For example, Barshilia et al. [21,22] prepared TiN/a-C composite films by DC reactive magnetron sputtering, which greatly improved the toughness and hardness of the films. MoS<sub>2</sub> has a layered structure similar to graphite, and the layers are only connected by a weak van der Waals force, which makes the MoS<sub>2</sub> weak in shear resistance and prone to interlayer slippage, which reduces the coefficient of friction [23,24]. In addition, a low MoS<sub>2</sub> has the advantages of a wide temperature range and an improved lubrication performance in anoxic environments and has been used as a coating material in the aerospace field [25,26], making it the most widely used solid coating material [27]. Voevodin et al. [28] prepared an MoS<sub>2</sub>-DLC nanocomposite film by pulsed laser deposition and proposed a new nanocomposite structure through the combination of crystalline carbide, diamond-like carbon (DLC) and transition metal chalcogenides. Therefore, the composite coating of a DLC/MoS<sub>2</sub> has great research value.

In order to improve the frictional properties of material surfaces, many researchers have started laser treatment of material surfaces to enhance friction performance and have achieved corresponding results. Conradi et al. [29] utilized a nanosecond laser on a Ti6Al4V alloy surface to process different morphologies and analyzed the effect of surface morphology, weave density and orientation on the frictional properties under dry and lubricated sliding conditions. Under dry conditions, the pits exhibited lower coefficients of friction, and under lubricated conditions, the lines and cross-shadows exhibited, after abrasion and the removal of bumps around the laser texture, better friction characteristics. Niu et al. [30] fabricated a series of pit weave surfaces with different geometrical parameters (area density, diameter and depth) on a medium-carbon steel surface. The friction and wear behavior of the textured surfaces during the wear process was analyzed by friction and wear tests, and it was found that the depth of the pits was the main factor affecting the friction and wear performance. Zhang et al. [31] showed the best tribological performance of the Al<sub>2</sub>O<sub>3</sub>/GNP-coated Al<sub>2</sub>O<sub>3</sub> composites by using an inductively coupled plasma etching (ICP) technique to prepare micro-weave configurations with precise parameters (width and area ratios) on a silicon substrate. It was found by orthogonal experiments that the area ratio had a more significant effect on the coefficient of friction compared to the width and the load. Yang et al. [32] fabricated volcano-shaped weaves on the surface of samples by a laser. For samples with different weave diameters or weave area ratios, it was found after friction experiments that the volcano-shaped weave with an appropriate diameter and area ratio is beneficial to reduce the coefficient of friction and adhesive wear, while the weave with a large area ratio increases the friction instead.

With the progress of research in recent years, more and more researchers are attempting to combine laser processing with solid coatings. LIU et al. [33] obtained lattice-textured alumina/GNP-coated Al<sub>2</sub>O<sub>3</sub>/TiC matrix composites by depositing alumina/Graphene Nanoparticle (GNP) coatings on Al<sub>2</sub>O<sub>3</sub>/TiC matrix composites, which were treated with lattices and lines for laser micro-weaving. TiC substrate composites exhibited the best tribological properties. Gateman et al. [34] demonstrated a low coefficient of friction and relatively high wear resistance compared to a single solid coating by compression molding a blend of solid lubricating polymer polytetrafluoroethylene (PTFE) and wear-resistant polymer polyimide (PRP) and depositing it onto the substrate by thermal spraying. Peng et al. [35] deposited the Al-25Si wear-resistant coating by the inner-hole supersonic plasma spraying technique, which significantly improved the wear resistance of the aluminum alloy cylinder liner. Niu et al. [36] investigated the effects of thermal oxidation and laser surface texturing on the tribological properties of Ti-Zr alloys. The results of orthogonal tests found that thermal oxidation significantly improved the tribological properties of the

surface, and the synergistic effect of thermal oxidation and laser surface weaving treatment can further improve the tribological properties. The crater texture can exist for a long time and provide effective lubrication. Liu et al. [37] combined laser surface texturing and plasma nitriding techniques to improve the tribological properties as well as the wear resistance of Zr-2.5Nb alloys by generating microtextured nitriding layers.

At present, for the surface modification of titanium alloys, most of the studies are still on a single coating material or a single fabric, and the tribological properties under the synergistic effect of fabric and coating have not been systematically investigated, which has a wide range of application prospects. The improvement of friction performance under dry friction conditions is limited by a single fabric, while a single coating is greatly affected by the environment or abrasive particles, so the combination of the two is of great research value. In this paper, rectangular microstructures were prepared on the surface of TC4 titanium alloy using picosecond laser technology, and interlayered composite nanocoatings of DLC/MoS<sub>2</sub> were prepared by magnetron sputtering. The friction and wear tests were carried out on single fabric, single coating and fabricated coating samples, and an electron microscope and a laser confocal microscope were used to study the effects of different surface conditions on their roughness, abrasion patterns, friction coefficients and wear amounts. The friction coefficients and abrasion patterns of the fabricated coatings were investigated for different friction durations and operating temperatures, on the basis of which the tribological properties of the coatings were analyzed. This work can provide theoretical and applied guidance for the long service life of high-performance alloys and the synergistic effect of fabrication and coating.

## 2. Experimental Section

### 2.1. The Preparation of Microtexture

The TC4 alloy plate was cut into several specimens with dimensions of 20 mm × 20 mm × 5 mm using wire cutting, and the surface of the specimens was ground and polished before laser processing. The picosecond ultraviolet laser processing system of Wuhan Yuanlu Optoelectronics Technology Co., Ltd. (Wuhan, China) was used to process the microtexture of the TC4 sample. The laser wavelength was 355 nm, the pulse width was 15 ps, the power was 15 W, the frequency was 200 kHz and the scanning speed was 500 m/s. The prepared pit texture was a rectangular texture with a side length of 80 μm, and the texture spacing was 200 μm.

### 2.2. The Preparation of Multilayer Composite Nanocoatings

Teer UDP-650 closed-field non-equilibrium magnetron sputtering equipment (Teer Coatings Ltd., Droitwich Worcestershire WR9 9AS, UK) was used to prepare DLC/MoS<sub>2</sub> multilayer composite nanocoatings on the surface of the textured sample. The deposition system has four symmetrically placed sputtering targets, two of which are MoS<sub>2</sub> targets and two of which are C targets. The substrates are textured TC4 titanium alloy and untextured TC4 titanium alloy. The textured TC4 titanium alloy is mainly used for friction and wear testing, and the untextured TC4 titanium alloy is mainly used for thin film analysis. The specific deposition steps are as follows: the deposited sample is ultrasonically cleaned with acetone (Teer Coatings Ltd., Droitwich Worcestershire WR9 9AS, UK) and absolute ethanol (Teer Coatings Ltd., Droitwich Worcestershire WR9 9AS, UK) for 30 min and dried with flowing nitrogen, and then the sample is clamped on the sample holder. Before thin film deposition, the vacuum chamber was pre-evacuated until the background vacuum degree was better than  $1.0 \times 10^{-3}$  Pa, high-purity argon gas (purity 99.999%) was introduced, a  $-500$  V bias was applied to the sample holder, and glow discharge etching was used to remove oxides and other contaminants on the sample surface. The alternate deposition of composite films is controlled by alternately adjusting the start and stop times of the sputtering target; the sputtering time of the C target is fixed at 40 s. By adjusting the sputtering time of the MoS<sub>2</sub> target, a DLC/MoS<sub>2</sub> nanometer multilayer film is prepared,

as shown in Figure 1 which indicates repeat operation. The magnetron sputtering process parameters are shown in Table 1.

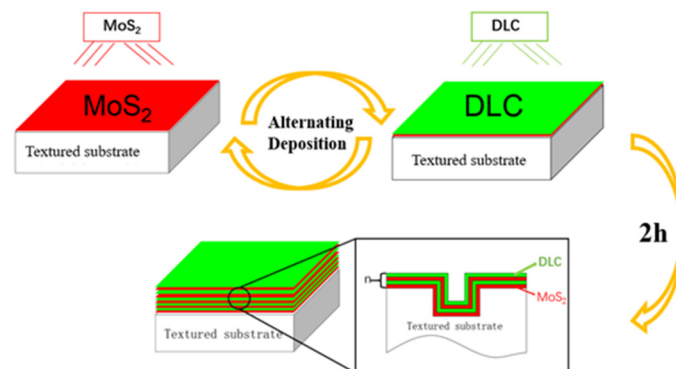


**Figure 1.** Schematic diagram of preparation of multilayer composite nanocoating.

**Table 1.** Magnetron sputtering process parameters.

Target	Magnetron Time (s)	Magnetron Current (A)
MoS <sub>2</sub>	40	0.8
DLC	40	0.6

### 2.3. Characterization of Structure and Properties of Textured Multilayer Composite Coatings

The roughness and morphology of the multilayer composite nanocoating were measured and observed using an Osparin OLS4000 laser confocal microscope (OLYMPUS, Tokyo, Japan). The cross-section of the coating was observed and characterized using an FEI Quanta 650FEG scanning electron microscope (FEI Company, Eindhoven, the Netherlands). The surface hardness of the composite nanocoating was measured using an EM-1500L microhardness tester. The NANOVEA T50 “ball-disk” multifunctional friction and wear testing machine was used to study the synergy between a single texture, a single composite coating, and the microtexture and composite coating at a relative humidity of 40% and a temperature of 25 °C. A 304 stainless steel ball with a diameter of 6 mm was selected as the counter friction material. The friction test was carried out under a constant load of 4 N, a sliding stroke of 10 mm, a sliding speed of 20 mm/s, a sliding time of 15 min and a number of reciprocating cycles of 900 times. The wear amount of the textured multilayer composite nanocoating can be measured by scanning the cross-sectional area of the wear scar using an OLS4000 laser confocal microscope. After the friction test, a scanning electron microscope (SEM) was used to observe the surface micromorphology of the sample and the dual steel ball, and an energy dispersive spectrometer (EDS) was used to analyze the composition of the wear debris on the surface of the steel ball. In addition, the tribological properties of textured composite nanocoatings under different friction cycles (such as Table 2) and different temperatures (such as Table 3) were also studied.

**Table 2.** Friction test parameters under different friction cycles.

Working Condition	Load (N)	Sliding Speed (mm/s)	Sliding Stroke (mm)	Sliding Period	Sliding Duration (min)
1	4	20	10	900	15
2				1800	30
3				3600	60
4				7200	120

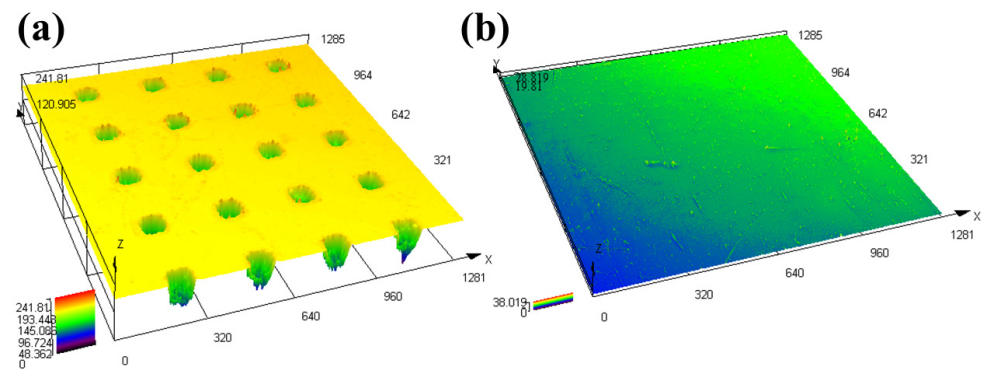
**Table 3.** Friction test parameters at different temperatures.

Working Condition	Load (N)	Sliding Speed (mm/s)	Sliding Stroke (mm)	Sliding Period	Temperature (°C)
1	4	20	10	900	25
2					100
3					150
4					200

### 3. Results and Discussions

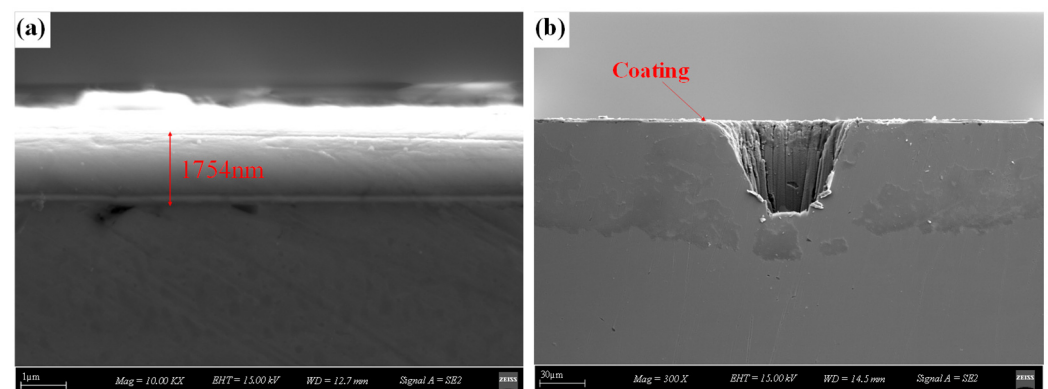
#### 3.1. Microstructure and Mechanical Properties of Textured Multilayer Composite Nanocoatings

The surfaces of the composite coating and the textured composite coating were observed using a laser confocal microscope, and the roughness was measured as shown in Figure 2. Figure 2a shows the surface morphology of the textured composite coating, and the average roughness measured is 2.358  $\mu\text{m}$ . Figure 2b shows the surface morphology of the composite coating, and the average roughness measured is 0.312  $\mu\text{m}$ . It can be seen that the microtexture will increase the roughness of the surface to a certain extent.



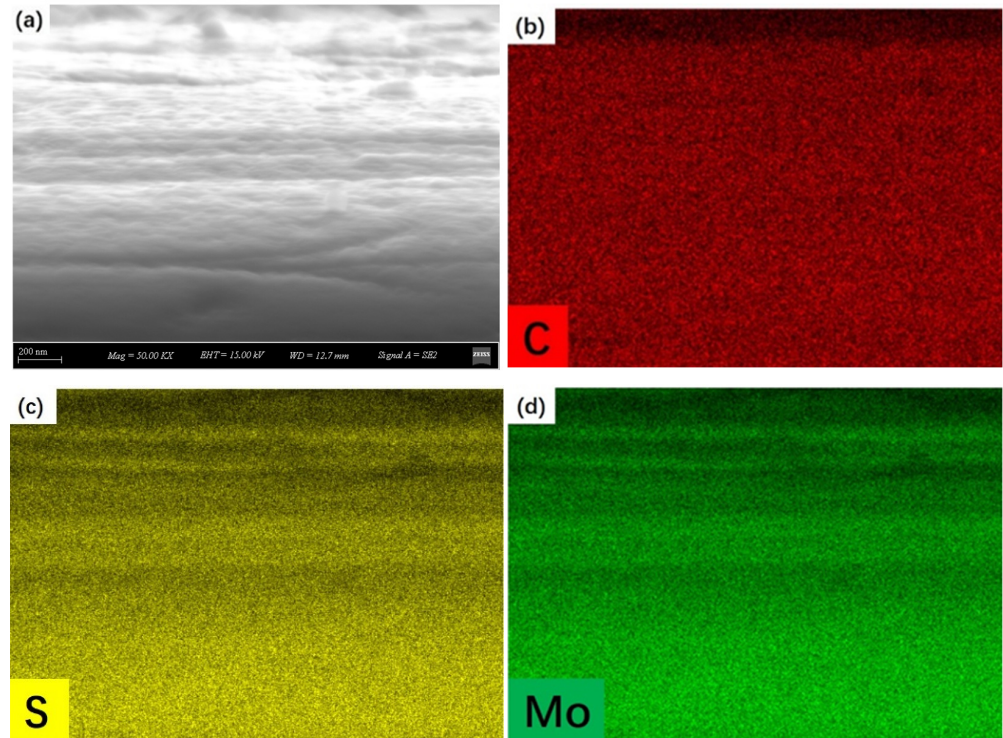
**Figure 2.** The surface morphology of the DLC/MoS<sub>2</sub> composite nanocoating for the (a) textured coating; (b) the coating was observed by an ols4000 laser confocal microscope.

Figure 3a shows the cross-sectional SEM image of the multilayer composite nanocoating. The thickness of the composite coating can be measured to be  $1754 \pm 1$  nm. The rectangular microtexture shown in Figure 3b is an inverted trapezoid with a certain slope on the edge. The multilayer composite nanocoatings mainly exist on the surface of textures, and the geometric shape inside the rectangular texture causes shadow effects, reducing the direct irradiation of the sputtering source on the internal area, thereby affecting the deposition texture of the coating. There is no composite coating sputtered inside the texture.



**Figure 3.** The cross-section morphology of DLC/MoS<sub>2</sub> composite nanocoatings for (a) composite coating cross-section and (b) cross-section of textured composite coating by SEM.

An EDS energy spectrum analyzer was used to conduct an energy spectrum scan of the multilayer composite nanocoating. As shown in Figure 4, it can be seen that the C, S and Mo elements are mainly distributed in the composite coating, and the element distribution has obvious overlap.



**Figure 4.** Element distribution of multilayer composite nanocoatings for (a) composite coating area; (b) C element; (c) S element; and (d) Mo element by EDS.

The EM-1500L microhardness tester was used to measure the microhardness of the composite coating surface. As shown in Figure 5, the average microhardness measured at any five positions on the surface of the multilayer composite nanocoating was 511.72 HV, while the average microhardness of the TC4 surface was 223.44 HV. It can be seen that the multilayer composite nanocoating has the characteristics of high hardness and can improve the wear resistance of the material surface.

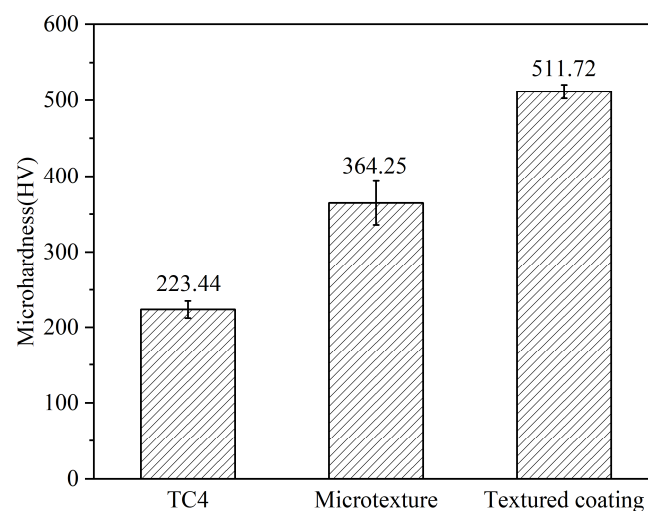


**Figure 5.** Microhardness of different samples.

### 3.2. Influence of Different Conditions on Friction Coefficient

#### 3.2.1. Effect of Surface Conditions on Tribology

The friction coefficient curves of a single texture, a single DLC/MoS<sub>2</sub> multilayer composite nanocoating, and a textured DLC/MoS<sub>2</sub> multilayer composite nanocoating at 4 N, friction speed 20 mm/s and friction time 15 min are shown in Figure 6. Stage I is the wear scar formation stage, and Stage II is the wear scar stabilization stage. The single textured surface is greatly affected by the experimental conditions, and the texture wears severely under reciprocating motion conditions [38] with a friction coefficient of around 0.4122 and significant fluctuations in friction coefficient. The surface of the coating and the surface of the textured coating benefit from the action of the nanocoating, and the friction coefficient remains stable at around 0.1094 and 0.0978 after the friction cycle reaches 400, which is much lower than that of the textured surface, and the fluctuation of the friction coefficient is relatively small. The friction coefficient of the coating surface gradually increases in the early stage of wear, and the smooth coating surface itself experiences coating wear and detachment in the early stage of wear. The detached coating powder forms small abrasive particles, causing the initial friction coefficient to increase. As the friction enters a stable phase, the friction coefficient remains at a relatively small level. Compared to smooth surfaces, textured coatings can capture wear particles due to the capture effect of microtextures [39,40]. Therefore, there is no significant increase in friction coefficient during the initial stage of wear, and a low friction coefficient level with minimal fluctuations can be maintained.

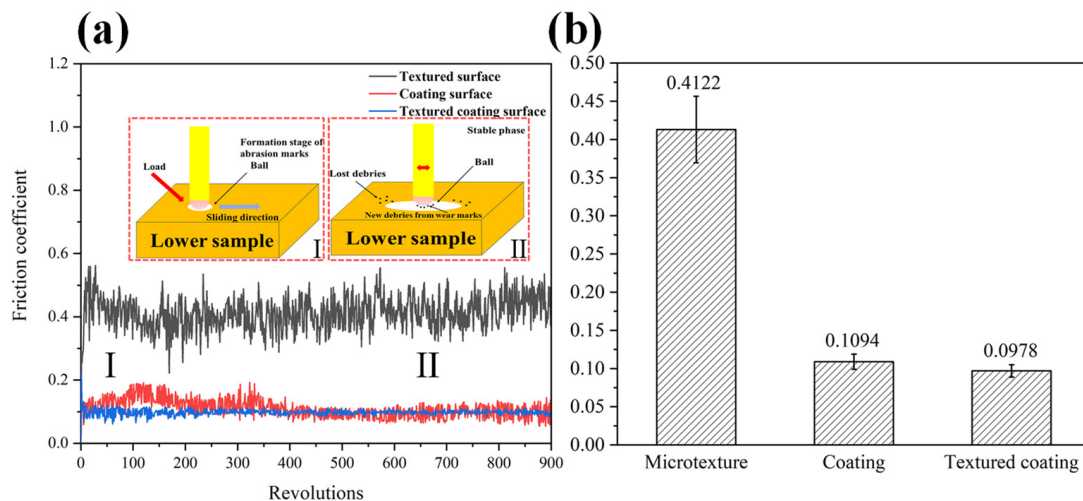


**Figure 6.** (a) Friction coefficient curve and (b) average friction coefficient of different samples.

Figure 7 shows the three-dimensional morphology and cross-sectional area of the wear scars of different samples. Figure 7a shows the three-dimensional morphology of the wear scars under a single microtexture, and obvious wear can be seen. Figure 7b,c are the three-dimensional morphology of the wear scars of single coating and textured coating samples, respectively. The wear is significantly reduced after preparing the composite coating. Figure 7d uses the average cross-sectional area of wear marks to represent the wear amount of different samples. The wear area of the single coating is around 11.456  $\mu\text{m}^2$  and the wear area of the substrate after the preparation of the interlayer composite coating is around 4.925  $\mu\text{m}^2$ , which is about a 57% reduction in the amount of wear. This indicates that there is a synergistic effect between the weave and the composite coating to reduce the wear more effectively and improve the wear resistance of the substrate.

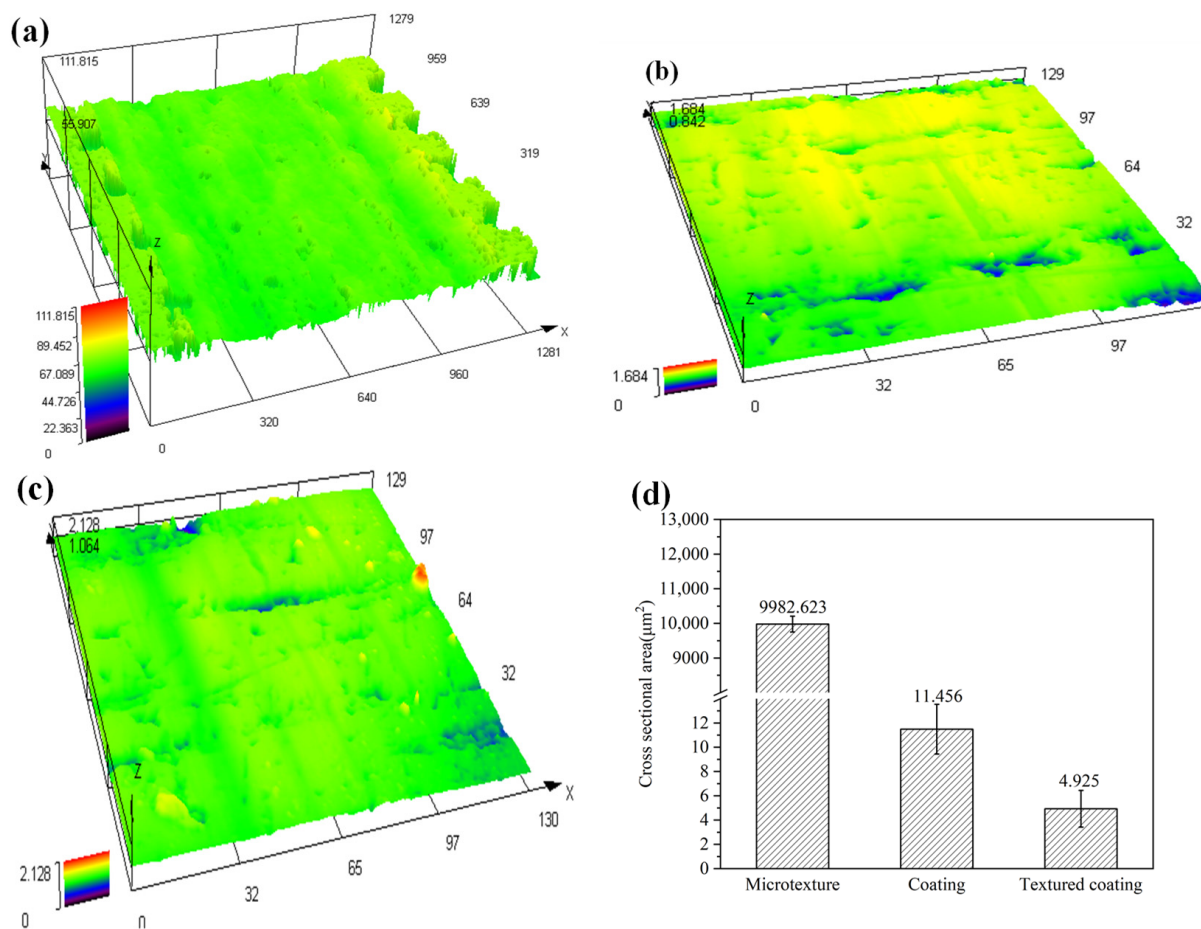


**Figure 7.** Wear trace morphology of different samples for (a) microtexture; (b) coating; (c) textured coating by Olympus OLS4000; and (d) cross-sectional area of wear mark.

### 3.2.2. Effect of Friction Duration on Friction Coefficient

Figure 8 shows the average friction coefficient of the textured coating surface under different friction cycles. It can be seen that the friction coefficient has a decreasing trend as the friction cycle increases. When the friction periods are 900, 1800, 3600 and 7200 revolutions, the average friction coefficients are 0.09781, 0.08394, 0.08343 and 0.06883, respectively. It can be seen that the textured coating can still maintain a good lubrication effect under high friction cycles. According to the wear theory, the influence of the friction coefficient will be affected by the change in three friction components, namely, adhesion, ploughing of wear particles, and deformation of the rough surface [41]. The composite coating surface itself initially has a certain degree of roughness, and its rough surface under the high friction cycle is gradually smoothed out to make the friction coefficient show a decreasing trend. At the same time, the accommodation of abrasive chips by the weaving structure during the friction process reduces the ploughing influence of the coating wear particles and reduces the three-body wear [42,43] of the abrasive chips and the friction contact surface.

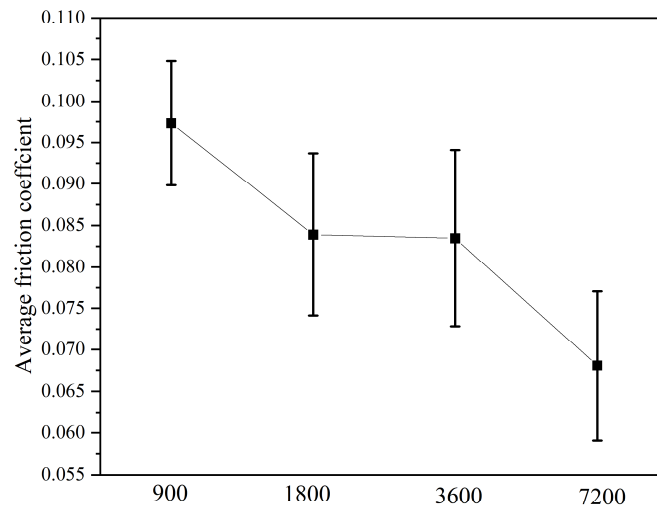


**Figure 8.** Average friction coefficient under different friction cycles.

### 3.2.3. Effect of Friction Temperature on Friction Coefficient

The textured coating samples were subjected to friction and wear tests at different temperatures to obtain the average friction coefficient versus a temperature curve, as shown in Figure 9. The coefficient of friction in the friction test at 25 °C was 0.0978; the coefficient of friction decreased to 0.07065 and 0.04673 when the temperature increased to 100 °C and 150 °C, respectively; and the coefficient of friction slightly increased to 0.05112 when the temperature continued to increase to 200 °C. It can be seen that the textured composite coating always exhibits a lower friction coefficient at different temperatures, and as the temperature increases, the friction coefficient first decreases and then increases. The friction coefficient is the smallest at a temperature of 150 °C. When the temperature exceeds 150 °C, the friction coefficient shows an upward trend, but the friction coefficient is still smaller than that at a normal temperature. The curves of the average friction coefficient at different temperatures illustrate that the textured composite coating still has good friction performance in high-temperature environments.

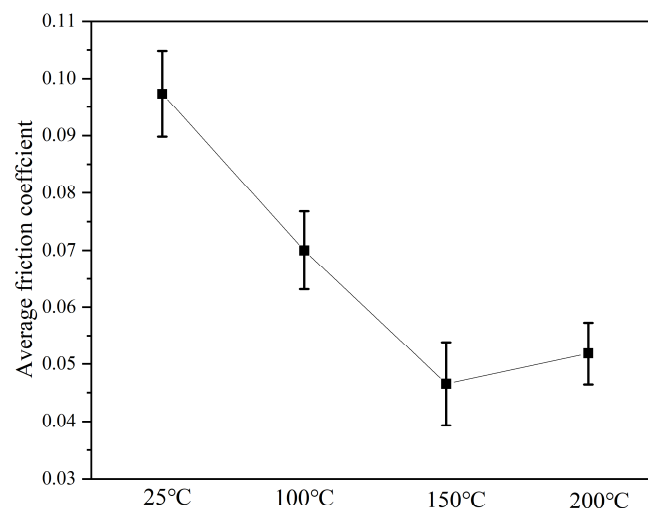


**Figure 9.** Average friction coefficient at different friction temperatures.

## 3.3. Wear Trace Morphology of Samples under Different Conditions

### 3.3.1. Wear Trace Morphology of Samples under Different Surface Conditions

Figure 10 shows the wear scar surfaces of different samples. In Figure 10a, the wear scars on the textured surface show relatively severe wear scars and matrix peeling caused

by adhesive wear, and the texture wear deformation is serious in the friction area. As shown in Figure 10b,c, the surface of the composite coating shows lighter adhesive wear and very little wear. This is because the hardness of the composite nanocoating is much greater than the base material, so the wear is lighter during the friction process. It can be seen from Figure 10c that the deformation of the fabrics under the same working conditions is greatly reduced after the preparation of the composite interlayer nanocoatings compared to the fabricated surface, indicating that the composite coatings are effective in prolonging the life of the fabrics and thus the friction and wear reduction properties of the fabrics.

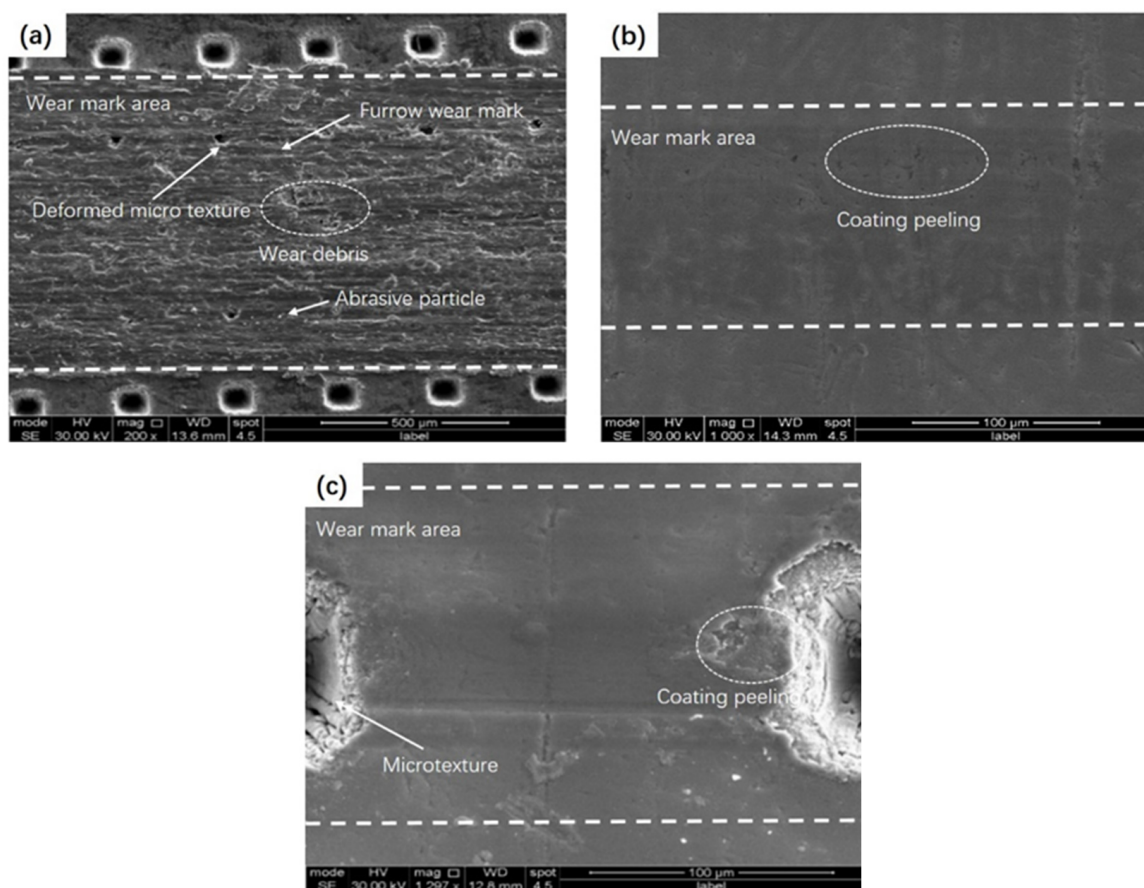


**Figure 10.** Wear mark surface of different samples for (a) microtexture; (b) coating; and (c) textured coating by SEM.

The weaving composite coating specimen had a large amount of debris in the micro-weave pits in the wear mark area (Figure 11), and the elemental composition of the debris was analyzed using an EDS to find that the debris contained elements such as Fe, S and C. The elemental analysis using the EDS proved that the abrasive debris was produced by the detachment of the dyadic steel balls as well as the composite coating. This also shows that the weave can indeed capture wear particles during friction and reduce the wear effect, thus reducing the coefficient of friction.

Observation and analysis of the wear scar surface of dual steel balls with single coating and textured coating (Figure 12) found that the steel ball showed obvious abrasive wear and slight adhesive wear, and black can be seen in the wear scar area as wear debris. The wear range of the dual steel ball of the single coated sample is smaller in comparison. This is because the existence of the texture causes part of the steel ball to sink into the pit when it passes through the pit, and the part that sinks in passes over the edge of the pit. This expands the contact range and leads to an increase in the wear scar area. In Figure 12b,d, it can be seen that, in addition to the Fe element itself, there is also the S element in the coating

on the surface of the steel ball, indicating that the composite coating forms a transfer film during the friction process, resulting in the transfer of elements in the coating. This also explains the ability of the nanocoatings to improve the substrate friction performance by means of solid lubrication, shown in Figures 6 and 7.

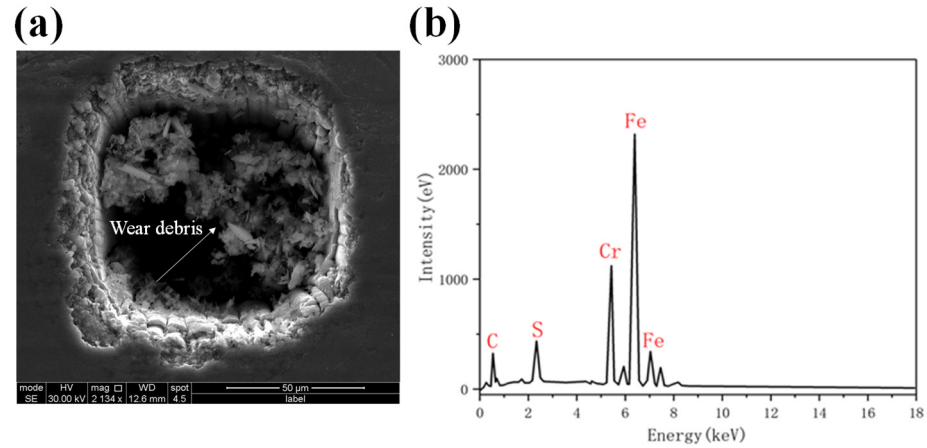


Figure 11. Texture region in textured composite coating by SEM and EDS for (a) microtexture pit and (b) EDS pattern of wear debris.

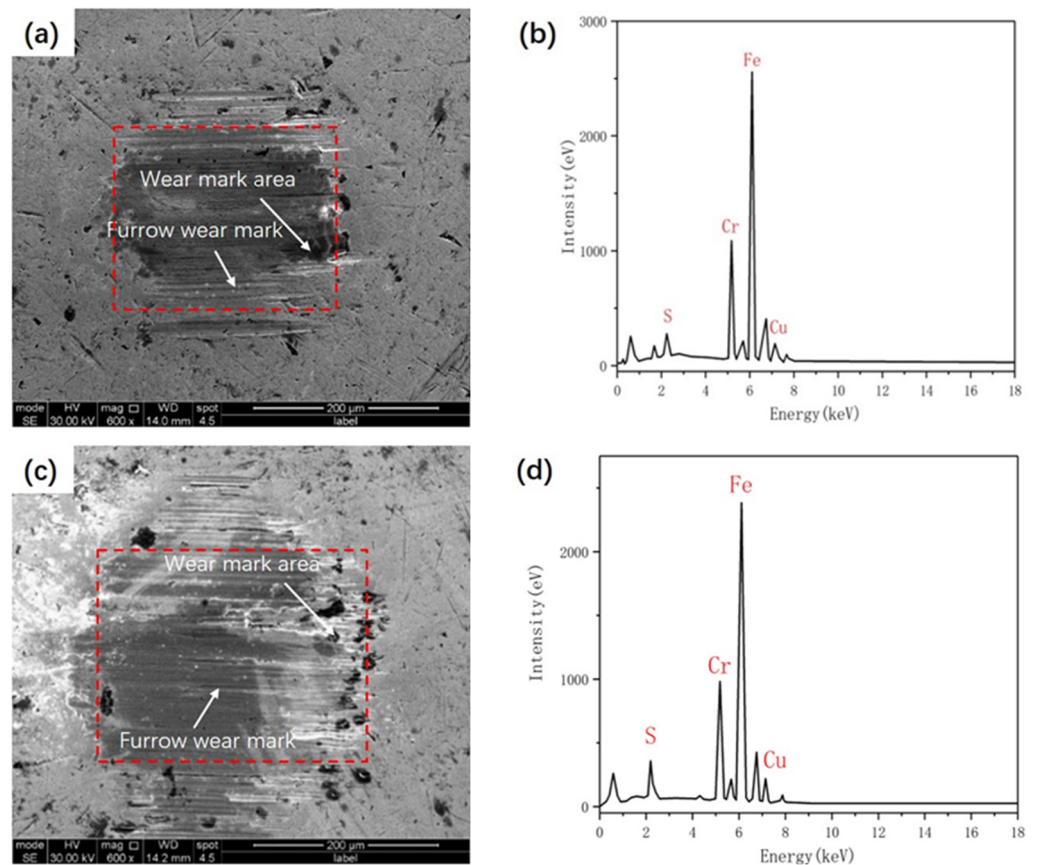
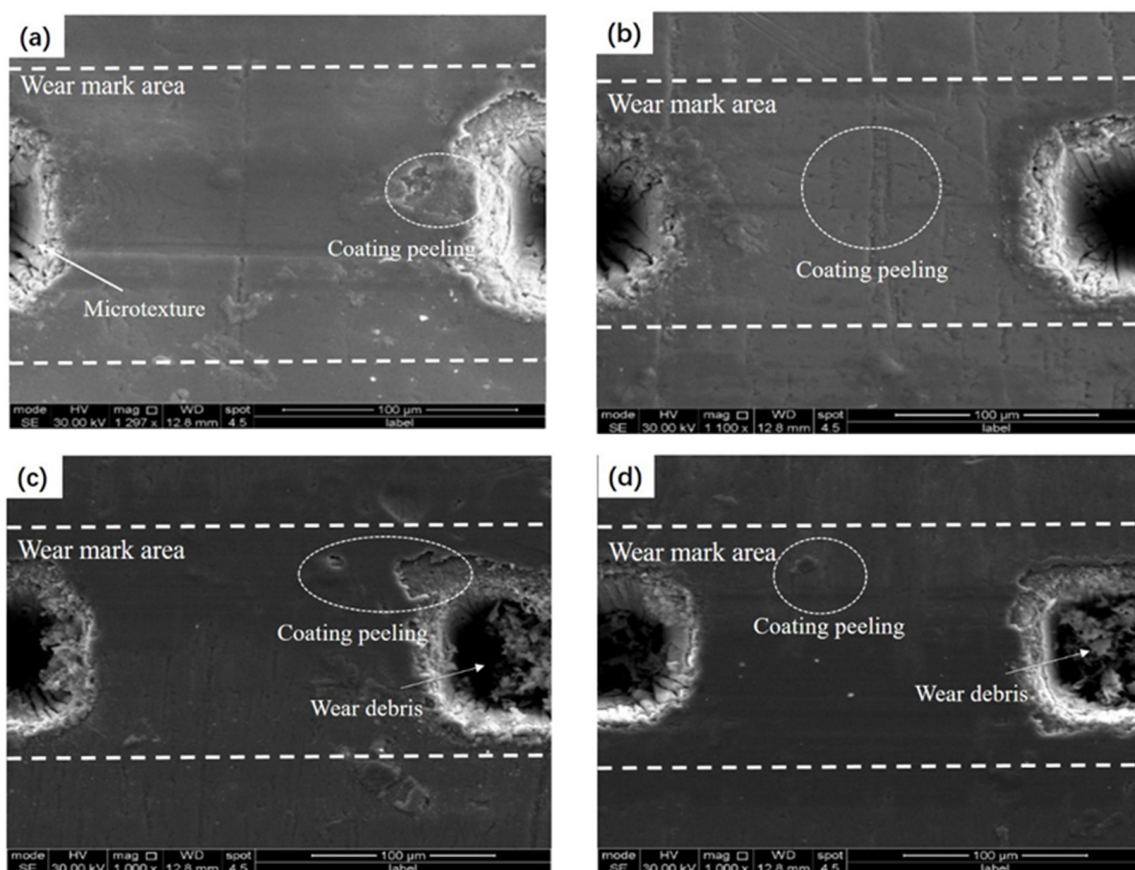


Figure 12. The surface micrograph of the ball by SEM for (a) steel ball in contact with coating and (b) steel ball in contact with textured coating; EDS pattern for (c) coating wear mark areas and (d) textured coating wear mark areas.

### 3.3.2. Wear Trace Morphology of Samples under Different Friction Duration

By using a scanning electron microscope to observe the abrasion areas at 900, 1800, 3600 and 7200 friction cycles, respectively, as shown in Figure 13, when the friction cycle is 900, it can be seen that the abrasion areas have some raised or concave areas, which lead to higher friction coefficients when the friction cycle is lower. As the friction cycle rises, the surface structure increases the contact area between the coating and the substrate, and at the same time, the use of the ‘mechanical interlocking’ structure improves the adhesion between the substrate and the coating, preventing the coating from falling off during friction [44], meaning the friction cycle in the 1800–3600 range within the friction coefficient is always maintained at a stable level. With the further increase in the friction cycle, when the friction cycle reaches 7200, it can be seen that the abrasion marks on the surface of the tiny peaks are smoothed out to make the abrasion mark area more and more flat. The reduction in roughness leads to a reduction in the coefficient of friction, and at the same time, the surface layer of the coating wear and tear after consumption, stored in the titanium alloy surface weave of the groove of the solid lubricant, can play a ‘self-compensatory’ effect, which explains the ability of the textured coating to maintain a low coefficient of friction over long friction cycles.



**Figure 13.** Wear trace morphology of samples under different friction cycles of (a) 900; (b) 1800; (c) 3600; and (d) 7200.

From the analysis of the coefficient of friction and wear marks, it can be concluded that the woven composite nanocoatings are effective in achieving good lubrication under long friction cycles. This is because the composite nanocoating has high hardness and a low coefficient of friction, which makes it less prone to wear at high friction cycles. The existence of microstructures can effectively reduce the large amount of abrasive debris generated in the high friction cycle, reducing the generation of abrasive wear and preventing wear intensification. At the same time, the nano-abrasive debris accommodated by the texture

through the capture effect can continue to play a solid lubrication role after the surface coating is worn out. Therefore, long-life lubrication can be achieved through the synergistic effect of fabrics and composite nanocoatings.

### 3.3.3. Wear Trace Morphology of Samples at Different Friction Temperatures

As shown in Figure 14, the different temperatures under the weaving structure of the coating specimen wear mark morphology, from Figure 14 a to c, can be seen in the weaving structure of the surface and can still maintain a relatively intact rectangular structure, and if the temperature is lower than the surface of its wear marks, it can still be relatively smooth. The increase in temperature promotes the precipitation of more  $\text{MoS}_2$ , which covers the surface of the material and is more conducive to the formation of a lubricating transfer film [45]; so, when the temperature rises, the coefficient of friction shows a downward trend. When the temperature is  $200\text{ }^\circ\text{C}$ , the wear is most serious, which also explains the reason why the friction coefficient rises after  $150\text{ }^\circ\text{C}$ . The wear of woven composite coatings will intensify with the increase in temperature, and some coatings will peel off in high-temperature environments, making the surface rough and uneven—generating a certain amount of debris (as shown in Figure 14d). The generation of debris further leads to the intensification of adhesive wear. This further explains the elevated coefficient of friction at high temperatures in Figure 9.

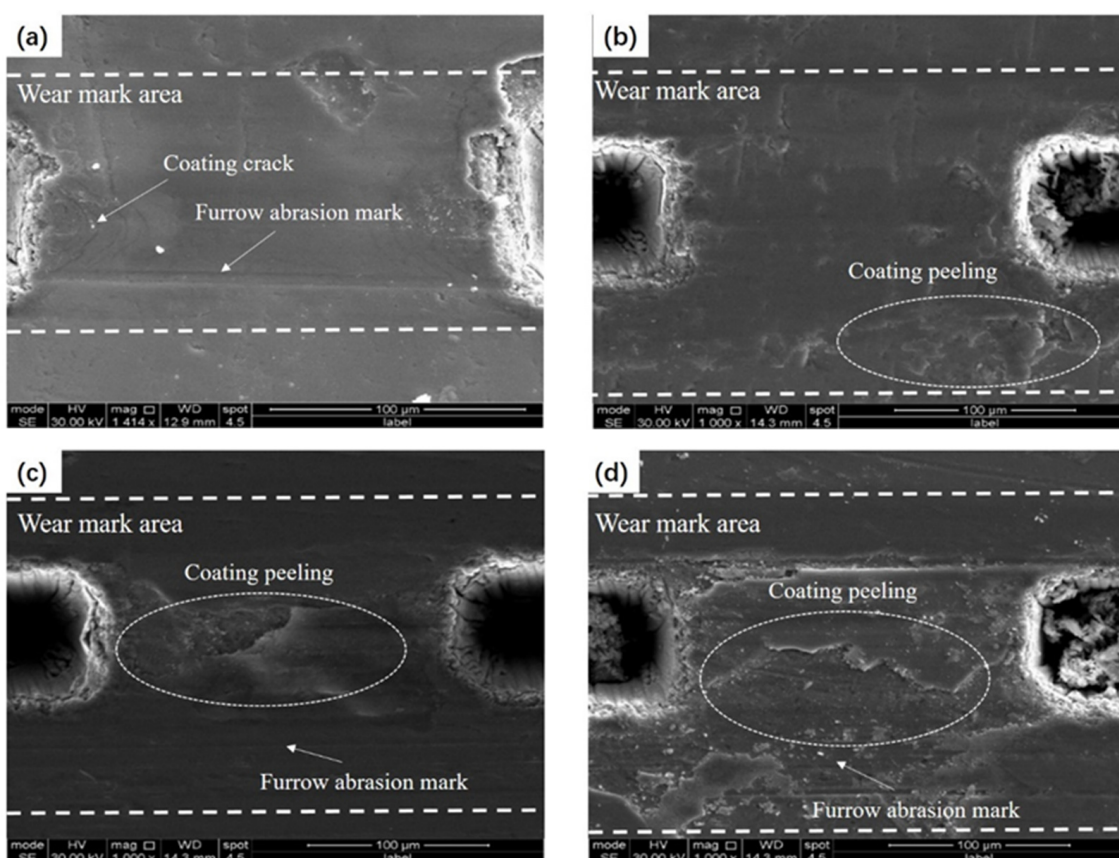


**Figure 14.** Wear trace morphology of samples at different friction temperatures of (a)  $25\text{ }^\circ\text{C}$ ; (b)  $100\text{ }^\circ\text{C}$ ; (c)  $150\text{ }^\circ\text{C}$ ; and (d)  $200\text{ }^\circ\text{C}$ .

## 4. Conclusions

- (1) Under the same friction conditions, the average friction coefficients of the three coatings were 0.4122, 0.1094 and 0.0978. Through the EDS analyses of the dyadic spheres and the abrasion mark area, the coatings produced certain abrasive debris during the friction process, which could form a stable transfer film during the friction process

thanks to the good lubrication performance of the nanocoatings, thus maintaining a very low friction coefficient. Meanwhile, the trapping effect of the woven texture on the abrasive debris makes the fluctuation of the friction coefficient smaller after the treatment of the woven coating.

- (2) The high hardness characteristics of multilayer composite nanocoatings result in minimal deformation of the texture during friction. Combined with the capture effect of microtextures on debris, the textured coating has the lowest wear under the same conditions and the best wear resistance.
- (3) In the long cycle friction experiment of textured coatings, the textured composite coating still has an extremely low friction coefficient and less wear under high friction cycles (7200 cycles) and has the characteristics of long-life lubrication.
- (4) Textured composite coatings can achieve low friction coefficients at a high temperature (200 °C), but their wear resistance has decreased. As the temperature increases, the friction coefficient of the textured coating shows a trend of first decreasing and then increasing, but all values remain relatively low.

**Author Contributions:** Conceptualization, K.L. and N.K.; methodology, Q.D.; software, Q.D.; validation, X.X., H.P., K.G. and M.L.; formal analysis, K.L.; investigation, X.X.; resources, K.G., H.P.; data curation, X.X.; writing—original draft preparation, Q.D.; writing—review and editing, Q.D. and N.K.; visualization, Q.D.; supervision, K.L.; project administration, N.K.; and funding acquisition, K.L. All authors have read and agreed to the published version of the manuscript.

**Funding:** This research was funded by the Scientific Research and Technology Development Project of China National Petroleum Corporation, “Development of Active Control Equipment for Wellbore Cooling at 50 °C”, grant number 2024ZG28; the scientific research and technology development project of the China National Petroleum Corporation’s Engineering Technology Research Institute Co., Ltd., grant number CPET202320; and the research on the “thermal-structure” coupling mechanism and the new materials of the dynamic seal pair of the compressor module of the downhole active cooling device, grant number NERCDCT202307.

**Data Availability Statement:** Data is contained within the article or supplementary material.

**Conflicts of Interest:** Author Ke Liu, Hao Peng, Kang Guan, Xiaowan Xi were employed by CNPC Engineering Technology R & D Company Limited and National Engineering Research Center of Oil & Gas Drilling and Completion Technology. The remaining authors declare that the research was conducted in the absence of any commercial or financial relationships that could be construed as a potential conflict of interest.

## References

1. Li, H.; Zhou, H.; Zhang, D.; Zhang, P.; Zhou, T. Influence of varying distribution distance and angle on fatigue wear resistance of 40Cr alloy steel with laser bionic texture. *Mater. Chem. Phys.* **2022**, *277*, 125515–125525. [[CrossRef](#)]
2. Vidyasagar, K.E.C.; Pandey, R.K.; Kalyanasundaram, D. Improvement of Deep Groove Ball Bearing’s Performance Using a Bionic Textured Inner Race. *J. Bionic Eng.* **2021**, *18*, 974–990. [[CrossRef](#)]
3. Hou, Q.; Yang, X.; Cheng, J.; Wang, S.; Duan, D.; Xiao, J.; Li, W. Optimization of Performance Parameters and Mechanism of Bionic Texture on Friction Surface. *Coatings* **2020**, *10*, 171. [[CrossRef](#)]
4. Huang, Q.; Shi, X.; Xue, Y.; Zhang, K.; Gao, Y.; Wu, C. Synergetic effects of biomimetic microtexture with multi-solid lubricants to improve tribological properties of AISI 4140 steel. *Tribol. Int.* **2022**, *167*, 107395–107409. [[CrossRef](#)]
5. Zhan, X.; Liu, Y.; Yi, P.; Yin, X.; Fan, C.; Ma, J. Parameter-dependent tribological properties of sinusoidal-textured plasma-sprayed coatings. *Tribol. Int.* **2022**, *174*, 107738–107749. [[CrossRef](#)]
6. Li, S.; Chen, H.; Luo, T.; Xiao, G.; Yi, M.; Chen, Z.; Zhang, J.; Xu, C. Tribological properties of laser surface texturing modified GCr15 steel under graphene/5CB lubrication. *J. Mater. Res. Technol.* **2022**, *18*, 3598–3611. [[CrossRef](#)]
7. Mutyala, K.C.; Wu, Y.A.; Erdemir, A.; Sumant, A.V. Graphene-MoS<sub>2</sub> ensembles to reduce friction and wear in DLC-Steel contacts. *Carbon* **2019**, *146*, 524–527. [[CrossRef](#)]
8. Liu, N.; Liu, Q.; Bai, Y.; Sun, Y.; Li, Z.; Bao, M.; Zhan, H.; Guo, D.; Ma, Y. Tribological behavior of plasma-sprayed metal based solid self-lubricating coatings under heavy load. *Wear* **2021**, *486–487*, 204108–204117. [[CrossRef](#)]
9. Yang, Y.; Zhu, J.; Hou, K.; Ma, L.; Li, Z.; Jia, W.; Wang, H.; Wang, J.; Yang, S. Friction-induced construction of PTFE-anchored MXene heterogeneous lubricating coating and its in-situ tribological transfer mechanism. *Chem. Eng. J.* **2022**, *442*, 136238–136248. [[CrossRef](#)]

10. Huang, Q.; Wu, C.; Shi, X.; Xue, Y.; Zhang, K. Synergistic lubrication mechanisms of AISI 4140 steel in dual lubrication systems of multi-solid coating and oil lubrication. *Tribol. Int.* **2022**, *169*, 107484–107495. [[CrossRef](#)]
11. Yan, M.; Wang, X.; Zhang, S.; Zhang, S.; Sui, X.; Li, W.; Hao, J.; Liu, W. Friction and wear properties of GLC and DLC coatings under ionic liquid lubrication. *Tribol. Int.* **2020**, *143*, 106067–106077. [[CrossRef](#)]
12. Yu, G.; Gong, Z.; Jiang, B.; Wang, D.; Bai, C.; Zhang, J. Superlubricity for hydrogenated diamond like carbon induced by thin MoS<sub>2</sub> and DLC layer in moist air. *Diam. Relat. Mater.* **2020**, *102*, 107668–107675. [[CrossRef](#)]
13. Tian, J.; Jin, J.; Zhang, C.; Xu, J.; Qi, W.; Yu, Q.; Deng, W.; Wang, Y.; Li, X.; Chen, X.; et al. Shear-induced interfacial reconfiguration governing superlubricity of MoS<sub>2</sub>-Ag film enabled by diamond-like carbon. *Appl. Surf. Sci.* **2022**, *578*, 152068–152081. [[CrossRef](#)]
14. Enke, K.; Dimigen, H.; Hübsch, H. Frictional-properties of diamond-like carbon layers. *Appl. Phys. Lett.* **1998**, *36*, 291–292. [[CrossRef](#)]
15. Dimigen, H.; Hübsch, H. Applying low-friction wear-resistant thin solid films by physical vapour deposition. *Phillips Tech. Rev.* **1983**, *41*, 186–197.
16. Wang, M.; Schmidt, K.; Reichelt, K.; Dimigen, H.; Hübsch, H. Characterization of metal-containing amorphous hydrogenated carbon films. *J. Mater. Res.* **1992**, *7*, 667–676. [[CrossRef](#)]
17. Wei, Q.; Sharma, A.; Sankar, J.; Narayan, J. Mechanical properties of diamond-like carbon composite thin films prepared by pulsed laser deposition. *Compos. Part B Eng.* **1999**, *30*, 675–684. [[CrossRef](#)]
18. Ajayi, O.O.; Kovalchenko, A.; Hersberger, J.G.; Erdemir, A.; Fenske, G.R. Surface damage and wear mechanisms of amorphous carbon coatings under boundary lubrication conditions. *Surf. Eng.* **2003**, *19*, 447–453. [[CrossRef](#)]
19. Gassner, G.; Patscheider, J.; Mayrhofer, P.H.; Šturm, S.; Scheu, C. Tribological properties of nanocomposite CrC<sub>x</sub>/a-C:H thin films. *Tribol. Lett.* **2007**, *27*, 97–104. [[CrossRef](#)]
20. Gassner, G.; Patscheider, J.; Mayrhofer, P.H.; Hegedus, E.; Tóth, L.; Kovacs, I.; Pécz, B.; Srot, V.; Scheu, C.; Mitterer, C. Structure of sputtered nanocomposite CrC<sub>x</sub>/a-C:H thin films. *J. Vac. Sci. Technol. B* **2006**, *24*, 1837–1843. [[CrossRef](#)]
21. Barshilia, H.C.; Surya, P.M.; Sridhara, R.D.V.; Rajam, K. Superhard nanocomposite coatings of TiN/a-C prepared by reactive DC magnetron sputtering. *Surf. Coat. Technol.* **2005**, *195*, 147–153. [[CrossRef](#)]
22. Barshilia, H.C.; Surya, P.M.; Aithu, P.; Rajam, K. Corrosion behavior of TiN/a-C superhard nanocomposite coatings prepared by a reactive DC magnetron sputtering process. *Trans. Inst. Met. Finish.* **2004**, *85*, 1–7.
23. Jiang, A.; Cao, X.; Wang, Z.; Ma, J.; Xiao, J.; Ma, S. Friction performance and corrosion resistance of MoS<sub>2</sub>/DLC composite films deposited by magnetron sputtering. *Results Phys.* **2021**, *25*, 104278–104287. [[CrossRef](#)]
24. Cheng, B.; Li, Y.C.; Qiu, M. Tribological properties of graphene/MoS<sub>2</sub> composite coatings in multiple environments. *Lubr. Eng.* **2021**, *46*, 66–73.
25. Zhao, S.; Li, J.; Wang, R.; Ye, Q.; Mai, Y. Tribological properties of defect-rich molybdenum disulfide/graphene oxide composite coating under various environments. *Vacuum* **2022**, *202*, 111125–111131. [[CrossRef](#)]
26. Zhou, L.; Ding, Y.; Cai, Z.B. Research on impact wear behavior of MoS<sub>2</sub>/C composite coating under different pairs of grinding pairs. *Lubr. Eng.* **2021**, *46*, 31–37.
27. Yang, Y.; Fan, X.; Yue, Z.; Li, W.; Li, H.; Zhu, M. Synergistic lubrication mechanisms of molybdenum disulfide film under graphene-oil lubricated conditions. *Appl. Surf. Sci.* **2022**, *598*, 153845–153853. [[CrossRef](#)]
28. Voevodin, A.A.; Zabinski, J.S. Supertough wear-resistant coatings with “chameleon” surface adaptation. *Thin Solid Film.* **2000**, *370*, 223–231. [[CrossRef](#)]
29. Conradi, M.; Kocijan, A.; Klobcar, D.; Podgornik, B. Tribological response of laser-textured Ti6Al4V alloy under dry conditions and lubricated with Hank’s solution. *Tribol. Int.* **2021**, *160*, 107049–107057. [[CrossRef](#)]
30. Niu, Y.; Pang, X.; Yue, S.; Bao, S.; Zhang, Y. The friction and wear behavior of laser textured surfaces in non-conformal contact under starved lubrication. *Wear* **2021**, *476*, 203723–203730. [[CrossRef](#)]
31. Zhang, Z.; Feng, W.; Lu, W.; Du, X. Preparation and tribological properties of micro-textured diamond/WS<sub>x</sub> coatings. *Surf. Coat. Technol.* **2020**, *403*, 126369–126378. [[CrossRef](#)]
32. Yang, J.; Fu, H.; He, Y.; Gu, Z.; Fu, Y.; Ji, J.; Zhang, Y.; Zhou, Y. Investigation on friction and wear performance of volcano-shaped textured PVD coating. *Surf. Coat. Technol.* **2022**, *431*, 128044–128056. [[CrossRef](#)]
33. Liu, C.; Sun, J.; Venturi, F.; Romero, A.R.; Hussain, T. Microstructure and wear performance of alumina/graphene coating on textured Al<sub>2</sub>O<sub>3</sub>/TiC substrate composites. *J. Eur. Ceram. Soc.* **2021**, *41*, 1438–1451. [[CrossRef](#)]
34. Gateman, S.M.; Alidokht, S.A.; Mena-Morcillo, E.; Schulz, R.; Chromik, R.R.; Kietzig, A.-M.; Parkin, I.P.; Mauzeroll, J. Wear resistant solid lubricating coatings via compression molding and thermal spraying technologies. *Surf. Coat. Technol.* **2021**, *426*, 127790–127800. [[CrossRef](#)]
35. Peng, Q.; Liu, M.; Huang, Y.; Zhou, X.; Ma, G.; Wang, H.; Xing, Z. Microstructure, Phase Composition, Mechanical Properties and Tribological Properties of Plasma Sprayed Al-25Si Wear-Resistant Coatings. *Surfaces* **2022**, *5*, 350–364. [[CrossRef](#)]
36. Niu, Y.; Pang, X.; Yue, S.; Wang, S.; Song, C.; Bao, S.; Zhang, Y. Improving tribological properties of Ti-Zr alloys under starved lubrication by combining thermal oxidation and laser surface texturing. *Wear* **2022**, *496–497*, 204279–204289. [[CrossRef](#)]
37. Liu, Y.; Yang, Y.; Dong, D.; Wang, J.; Zhou, L. Improving wear resistance of Zr-2.5Nb alloy by formation of microtextured nitride layer produced via laser surface texturing/plasma nitriding technology. *Surf. Interfaces* **2020**, *20*, 100638–100645. [[CrossRef](#)]
38. Zhao, L.; Zhang, B.; Liu, Y.; Liu, Y. State of the art for improving tribological performance based on of surface texturing technology. *Tribology* **2022**, *42*, 212–215.

39. Bathe, R.; Krishna, V.S.; Nikumb, S.K. Laser surface texturing of gray cast iron for improving tribological behavior. *Appl. Phys. A* **2014**, *117*, 117–123. [[CrossRef](#)]
40. Dumitru, G.; Romano, V.; Gerbig, Y.; Weber, H.; Haefke, H. Femtosecond laser processing of nitride-based thin films to improve their tribological performance. *Appl. Phys. A* **2005**, *80*, 283–287. [[CrossRef](#)]
41. Suh, N.P.; Sin, H.C. The genesis of friction. *Wear* **1981**, *69*, 91–114. [[CrossRef](#)]
42. Chalkiopoulos, M.; Charitopoulos, A.; Fillon, M.; Papadopoulos, C.I. Effects of thermal and mechanical deformations on textured thrust bearings optimally designed by a THD calculation method. *Tribol. Int.* **2020**, *148*, 106303. [[CrossRef](#)]
43. Wang, X.Y.; Li, S.Y.; Dai, Q.W.; Huang, W.; Wang, X.L. Research progress in coordinated optimization of lubrication and leakage for texture mechanical seals. *Surface Technol.* **2019**, *48*, 1–8.
44. Ma, Z.; Lei, Y.; Fan, H.Z.; Hu, T.C.; Zhang, J.X.; Song, J.J.; Hu, L.T. Preparation of tungsten disulfide phosphate coating on textured titanium alloy surface and its tribological properties at elevated temperatures. *Tribology* **2023**, *43*, 469–480.
45. Wong, S.K.; Lu, X.; Cotter, J.; Eadie, D.T.; Wong, P.C.; Mitchell, K.A.R. Surface and friction characterization of MoS<sub>2</sub> and WS<sub>2</sub> third body thin films under simulated wheel/rail rolling–sliding contact. *Wear* **2008**, *264*, 526–534. [[CrossRef](#)]

**Disclaimer/Publisher’s Note:** The statements, opinions and data contained in all publications are solely those of the individual author(s) and contributor(s) and not of MDPI and/or the editor(s). MDPI and/or the editor(s) disclaim responsibility for any injury to people or property resulting from any ideas, methods, instructions or products referred to in the content.